

# Experiments on suspension flow in open channels with bed forms

## Étude expérimentale d'écoulements en suspension dans un canal ouvert sur formes de fond

M. CELLINO\* and W.H. GRAF, *Laboratoire de Recherches Hydrauliques, Ecole Polytechnique Fédérale, Lausanne, Switzerland*

\* now engineer, Bonnard & Gardel Consulting, Lausanne, Switzerland

### ABSTRACT

The influence of bed forms in open-channel flow on the suspended sediment concentration distribution is experimentally studied. At one single measuring section the flow and the concentration profiles have been investigated in order to put the effect of bed forms into evidence. From these measurements the sediment- and momentum-diffusion coefficients, eq. 4, have been calculated; subsequently the  $\bar{\beta}$ -value, which appears in the Rouse relation, eq. 2, could be evaluated.

With these results it could be shown that the concentration distribution, given by the Rouse relation, is altered due to the presence of bed forms. The  $\bar{\beta}$ -value for suspension flow over bed form, being  $\bar{\beta} > 1$ , appears to be larger than the one for comparable suspension flow over a plane bed, being  $\bar{\beta} < 1$ . Also investigated is the evolution of the flow structure, measured along part of a bed form. The velocity distributions reveal a separating shear layer and a recirculating region. The turbulence and Reynolds-stress profiles show clear peaks in the vicinity of the shear layer.

*Keyword:* Open-channel flow, Suspension flow, bed forms, vertical concentration distribution, turbulence

### RÉSUMÉ

Une étude expérimentale de l'influence des formes de fond sur la distribution de la concentration de sédiments en suspension est décrite.

L'effet des formes de fond est étudié à l'aide de mesures de l'écoulement et de profils de concentration dans une section. Ces mesures ont permis le calcul du coefficient de diffusion des sédiments ainsi que l'évaluation du coefficient de diffusion de quantité de mouvement, eq. 4. Par conséquent la valeur de  $\bar{\beta}$  apparaissant dans l'équation de Rouse, eq. 2, a été estimée.

Les résultats montrent que la distribution de la concentration donnée par l'équation de Rouse, est modifiée par la présence des formes de fond. La valeur de  $\bar{\beta}$  pour les écoulements en suspension sur des formes de fond semble être supérieure à la valeur observée ( $\bar{\beta} > 1$ ) pour des écoulements en suspension sur un fond plat ( $\bar{\beta} < 1$ ). L'évolution de la structure de l'écoulement mesurée le long d'une partie des formes de fond est également présentée. La distribution de vitesse révèle une couche de séparation et une région de recirculation. Les profils de turbulence et de tension de Reynolds montrent des pics à la proximité de la couche de cisaillement.

### 1 Introduction

Free-surface flow over a mobile bed is usually accompanied by entrainment of sediment and by formation of bed forms; both in turn will influence the flow and its sediment carrying capacity. Here is proposed to study the influence of fixed bed forms on the suspended-load transport.

The bed forms of the mobile bed, appearing as dunes and mini dunes, consist of spatially periodic irregularities. Indicative and useful relationships – determined on an empirical basis – were proposed by Yalin (see Graf, 1984, p. 283); they are:

$$\frac{\lambda}{h} \approx 5 \quad \frac{\Delta H}{h} < \frac{1}{6} \quad (1)$$

where  $\lambda$  and  $\Delta H$  are respectively the bed-form length and height and  $h$  is the flow depth.

The main effect of bed forms on flow is a flow separation behind the bed-form crest; there the flow is spatially decelerating. In this region recirculation takes place and local enhancement of turbulence is usually observed. Consequently, an influence on the vertical distribution of the suspended sediment concentration in the presence of bed forms and in particular behind the bed-form crest is to be expected.

For steady and uniform flow the vertical distribution of the suspension concentration,  $\bar{c}_s(y)$ , according to the diffusion-convection theory by Rouse (see Graf, 1984, p. 173), is given by:

$$\frac{\bar{c}_s}{\bar{c}_{sa}} = \left( \frac{h-y}{y} \frac{a}{h-a} \right)^z \quad (2)$$

with the Rouse number,  $z$ , defined as:

$$z = \frac{v_{ss}}{\kappa u_*} \quad \text{or} \quad z' = \frac{v_{ss}}{\beta \kappa u_*} = \frac{z}{\beta} \quad (3)$$

where  $y$  represents the distance from the top of the sediment layer (see Fig. 1),  $h$  is the flow depth,  $a = 0.05h$  is the reference level where the reference concentration,  $\bar{c}_{sa}^m$ , is measured,  $v_{ss}$  is the settling velocity of the particles in still clear water,  $\kappa$  is the Karman constant – assumed to be  $\kappa = 0.4$  for clear-water and for suspension flows – and  $u_*$  is the shear velocity.

The  $\bar{\beta}$ -value in eq. 3 is the depth-averaged value of  $\beta$ , representing the ratio of the sediment-,  $\epsilon_s$ , and the momentum-diffusion coefficient,  $\epsilon_m$ ; its vertical distribution is:

$$\beta(y) = \frac{\epsilon_s(y)}{\epsilon_m(y)} = \frac{\overline{c'_s v'(y)} / \frac{\partial \bar{c}_s(y)}{\partial y}}{\overline{u' v'(y)} / \frac{\partial \bar{u}(y)}{\partial y}} \quad (4)$$

where  $\overline{c'_s v'(y)}$  is the sediment flux and  $\overline{u' v'(y)}$  is the turbulent flux. Subsequently a depth-averaged  $\bar{\beta}$ -value can be obtained:

$$\bar{\beta} = \frac{1}{h} \int_a^h \beta(y) dy \quad (5)$$

Revision received March, 1999. Open for discussion till February 28, 2001.

A set of data from the Rio Grande river, presented by Nordin and Dempster, 1963, has been evaluated by Cellino, 1998, who obtained (by best fitting) large  $\bar{\beta}$ -values,  $0.7 < \bar{\beta} < 5$ . Carefully performed experiments by Lyn, 1988, Sumer et al., 1996 and Cellino and Graf, 1997 under capacity (saturation) condition without the presence of bed forms, showed rather small  $\bar{\beta}$ -values,  $\bar{\beta} < 1$ . Consequently, it seems reasonable to think that the bed forms – usually present in river flows – are at least partially responsible for these large  $\bar{\beta}$ -values. The present study tries to shed some light onto this discrepancy.

In order to compute the  $\bar{\beta}$ -values, the sediment,  $\epsilon_s(y)$ , and the momentum,  $\epsilon_m(y)$ , diffusion coefficients have to be obtained. While studies on the diffusion coefficients have been done in the past (see Jobson and Sayre, 1970, p. 715, Coleman, 1970, p. 807), good measurements of the sediment diffusion coefficient are still a challenging task. It is particularly the direct determination of the sediment flux,  $c_s v'(y)$ , which poses an almost insurmountable problem. The recent development of the APFP sonar instrument (see Shen and Lemmin, 1996, and Shen 1997) has allowed us to make an interesting contribution along this line.

In our research, we shall accept the concentration distribution given with the relation of Rouse, eq. 2, and shall try to express the effect of bed forms through the depth-averaged  $\bar{\beta}$ -value. This implies that the flow over bed forms is quasi-uniform. It would of course be desirable to study the evolution of the flow structure, of the concentration distribution and consequently of the  $\bar{\beta}$ -value evolution over one or two entire bed forms. However, our measuring equipment, the APFP instrument, is limited to measure the concentration distribution at one single section only where we were able to make detailed measurements. Nevertheless we find it worthwhile to report also our measurements on evolution of the flow structure over a part of a bed form (see chap. 4); for hasty reader, this part of the paper could readily be skipped.

## 2 Experimental facilities and flow conditions

The measurements have been made in a recirculating tilting channel, 16.8[m] long and  $B = 0.60$ [m] wide. Sediments were added slowly to the uniform flow; the measurements started only after 4[h] of flow circulation when the presence of a sediment layer ( $\approx 2$  [mm] thick) on the bed is assured. The layer thickness, measured periodically ( $\approx 0.5$  [h]) using manual limnimeters, was reasonably constant in time. The measuring section (n° 9) is located 13[m] from the entrance of the channel where the flow is assumed to be established; all measurements were performed at the centerline of the cross section.

Three artificial plastic (PVC) bed forms have been fixed on the channel floor in vicinity of the measuring section (see Fig. 1). The bed-form length,  $\lambda$ , and height,  $\Delta H$ , have been calculated with eq. 1 and are given in Table 1. This artificial geometry was slightly modified, when sediment deposited downstream of the crest.

The velocity and concentration measurements have been made with a sonar instrument, the APFP. With this instrument one obtains the instantaneous velocities profile by measuring the back-scattered echo signals (see Lhermitte and Lemmin, 1994). The measured velocity appears to be the one of the water/

sediment mixture (see Shen, 1997 and Cellino, 1998, ch.3). In addition, by measuring the forward and backward echo signals an echo intensity is obtained (see Shen and Lemmin, 1996 and Shen, 1997) being indicative of the sediment concentration. To get this concentration a calibration – using the suction-sampling method – was performed. The sonar transducers of the APFP are placed in water-filled housings in contact with the water surface and the channel bed (see Fig. 1); the resulting flow perturbation is thus minimized.

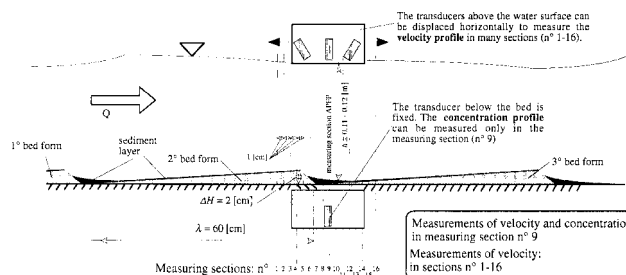


Fig. 1. Schematic of the bed forms.

The measurements were performed with the sediment-laden flow in capacity condition, notably when a layer of sediment, composed of the same sediment as is in suspension, is always present on the bed.

The measuring section (n° 9) was located between the second and third bed form, thus being close to the downstream face of a bed form. In this section the vertical transducer above the water surface is coaxial with the one below the bed. The vertical transducers operate alternatively emitting and receiving the ultrasonic echoes, which are proportional to the local suspension concentration. Since the transducer below the bed is fixed, thus it cannot be displaced, the APFP can be used to measure the concentration only in one single measuring section (n° 9). The point velocity,  $u(y, t)$ , and its corresponding concentration,  $c_s(y, t)$ , are extracted, with a frequency of 16 [Hz], from a cylinder-shaped measuring volume having a diameter of  $\Phi \approx 13$  [mm] and height of  $\Delta d \approx 5$  [mm] (see Shen, 1997, and Cellino, 1998) corresponding to a volume of nearly  $\text{Vol} \approx 7 \cdot 10^{-7}$  [m<sup>3</sup>]. For spherical-shaped sand particles of diameter  $d_{50} = 0.135$  [mm], a measuring volume contains  $\approx 26$  particles for  $c_s^m = 1$  [kg/m<sup>3</sup>] and up to  $\approx 130$  particles for  $c_s^m = 15$  [kg/m<sup>3</sup>]. In this measuring volume the instantaneous concentration and velocity are supposed to be homogeneous.

The velocity profile is obtained measuring the Doppler frequencies of the backscattered signals coming from the insonified water column. In a special configuration of the APFP instrument, the emitting and receiving transducers are all located in the housing above the water surface (the bed transducer is inactive during the velocity measurements). Thus, it was possible to displace horizontally the instrument. A tristatic configuration has been used to investigate the velocity profiles in many sections (n° 1-n° 16) along the bed forms. In the tristatic configuration the velocity measuring frequency could be increased up to 39 [Hz].

Two flows have been investigated, runs BF\_S015 and BF\_S02, whose hydraulic characteristics are summarized in Table 1. In addition, run BF\_S015 was repeated and a series of 16 velocity meas-

measurements around the bed-form crest have been performed to study the spatial evolution of the flow and its turbulence characteristics.

Table 1. Summary of data, for runs BF\_S015 and BF\_S02

Author	run	$Q$	$h$	$B/h$	$\lambda/h$	$\Delta H/h$	$U$	$S_f$	$Re \cdot 10^4$	$Fr$	$u_* \equiv u_{*c}$	$u_{*s}$
EPFL	BF_S015	0.038	0.110	5.5	5.5	0.18	0.575	0.150	6.322	0.55	0.032	0.040
EPFL	BF_S02	0.043	0.118	5.1	5.1	0.17	0.609	0.200	7.189	0.57	0.039	0.048

run	$d_{50}$	$\rho_s$	$v_{ss}$	$C_s^m$	$\bar{c}_{sa}^m$	$\bar{\rho}_m$	$\bar{\beta}_{SM}$ (best fit)	$\bar{\beta}_{APFP}$ (APFP)
BF_S015	0.135	2650	12.0	3.01	21.47	1001.87	1.347	1.142
BF_S02	0.135	2650	12.0	1.94	12.69	1001.21	1.113	1.116

The discharge,  $Q$ , has been evaluated as  $Q = U \cdot B \cdot h$ , where the depth-averaged velocity,  $U$ , is obtained by integrating over the depth the longitudinal velocity profile,  $\bar{u}(y)$ ; the flow depth,  $h$ , was measured using limnimeters. The flow depth,  $h$ , is the distance from the top of the sediment layer to the water surface (see Fig. 1). The aspect ratio,  $B/h$ , was high enough to consider the flow as bidimensional. The channel slope,  $S_f$ , refers to the bottom on which the artificial bed forms have been fixed. The Reynolds number,  $Re = U \cdot h/\nu$ , – where  $\nu$  is the cinematic viscosity of clear water – and the Froude number,  $Fr = U/\sqrt{g \cdot h}$ , show the flow to be turbulent and subcritical. The shear velocity,  $u_{*c}$ , has been obtained by extrapolating the Reynolds-stress distribution – measured in the upper part of the flow,  $y/h > 0.5$  – towards the bed (see Fig. 4e); this value represents a local estimation of the shear velocity. Subsequently, the shear velocity,  $u_{*s}$ , was also calculated using  $u_{*s} = \sqrt{ghS_f}$ . Both methods (especially the second one) are questionable for obvious reason, but for lack of a better method the shear velocity,  $u_*$ , used for any further calculation is taken as  $u_* \equiv u_{*c}$ .

The sediment used was sand having a characteristic diameter,  $d_{50} = 0.135$  [mm], and a density,  $\rho_s = 2650$  [kg/m<sup>3</sup>]. The settling velocity,  $v_{ss}$ , defined in still clear water, has been calculated (see Graf, 1984, p. 45). The depth-averaged concentration,  $C_s^m$ , and the reference concentration,  $\bar{c}_{sa}^m$ , have been measured with the suction method. The reference concentration,  $\bar{c}_{sa}^m$ , is evaluated at  $a = 0.05 \cdot h$ , which represents a vertical position in the flow. Defining  $a$  one implicitly assumes that above,  $y > a$ , the sediments are transported in suspension while below,  $y < a$ , the sediments are transported in bedload mode. Since the bedload layer exists only if the flow is in capacity condition, with such a definition of the reference concentration the resulting sediment transport as suspended load is in full capacity (saturation). The depth-averaged density,  $\bar{\rho}_m$ , is computed with the depth-averaged concentration.

The  $\bar{\beta}_{SM}$ -values have been obtained by best fitting eq. 2 – using the Rouse number defined in eq. 3 – to the measured dimensionless concentration distributions. Using the definition of eq. 4, the  $\beta(y)$ -values can be evaluated also experimentally using the data obtained with the APFP instrument. Subsequently the depth-averaged  $\bar{\beta}_{APFP}$ -values are obtained.

### 3 Velocity measurements

For both runs, BF\_S015 and BF\_S02, the measurement of the velocities and concentration profiles are obtained using the APFP instrument, positioned fixed in section n° 9 (see Fig. 1). The longitudinal

tudinal mean velocity profiles, in dimensional,  $\bar{u}$ [m/s], and in dimensionless form,  $\bar{u}/U$ , are plotted in Fig. 2a,b. They are compared to the velocity profiles measured in comparable plane-bed suspension flows (runs Q55S015 and Q60S02 refer to the same channel slope,  $S_f$ , while run Q40S003 had a similar discharge,  $Q$ ) which were reported in Cellino, 1998 ch. 3. The thick dashed gray line represents the height of the bed-form crest,  $\Delta H = 0.02$  (see Fig. 1). The thin gray lines represent the upper,  $y_{UV}$ , and lower level,  $y_{DV}$ , of the high vorticity region observed close to the bed-form crest (see Fig. 8a). In the upper part of the flow ( $y > y_{UV}$ ) all the profiles have similar tendencies while close to the bed ( $y < y_{UV}$ ), the ones measured in presence of bed forms fall to zero faster. Note the very small velocities close to the bed ( $y/h < 0.2$ ), which are probably due to the effect of the recirculating region within sections n° 7 and n° 9. Similar observations, both for the  $\bar{u}$  and  $\bar{v}$  profiles, have been communicated by Mendoza and Shen, 1990, p. 466, and Yoon and Patel, 1996, p. 15, performing mathematical models and by Lyn, 1993, p. 312, and Bennett and Best, 1995, p. 499, in experimental studies. In Fig. 2c the dimensionless vertical mean velocity profiles are shown. The high values of the downward vertical velocity (black symbols,  $\bar{v}/U \approx -0.07$ ) have to be associated to the reattachment of the flow to the bed behind the bed form. In case of comparable plane-bed suspension flow (gray symbols) the vertical velocities were smaller and usually directed upward.

The longitudinal and vertical components of the turbulence intensity plotted in Fig. 3a,b show the same trend as obtained by Yoon and Patel, 1996, p. 15, with a numerical model and by Nelson, McLean and Wolfe, 1993, p. 3942, in an experimental study. In particular, the presence of a peak close to the bed-form crest reveals the presence of a developing shear layer caused by the separation of the flow. For  $y > y_{UV}$  the magnitude of the both longitudinal and vertical component of the turbulence intensity (black points) is rather similar to the one observed in a comparable plane-bed suspension flows (gray points). Also the 16 profiles measured around the bed form show somehow the same tendency (see Fig. 4c,d).

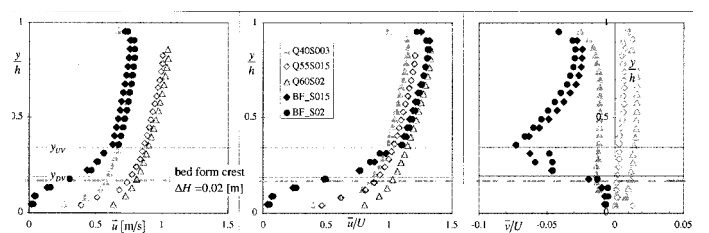


Fig. 2. a,b,c. Longitudinal and vertical mean velocity profiles, measured in section n° 9.

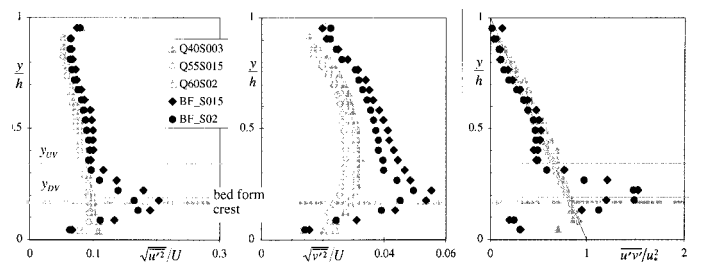


Fig. 3. a,b,c. Turbulence-intensity and Reynolds-stress profiles, measured in section n° 9.

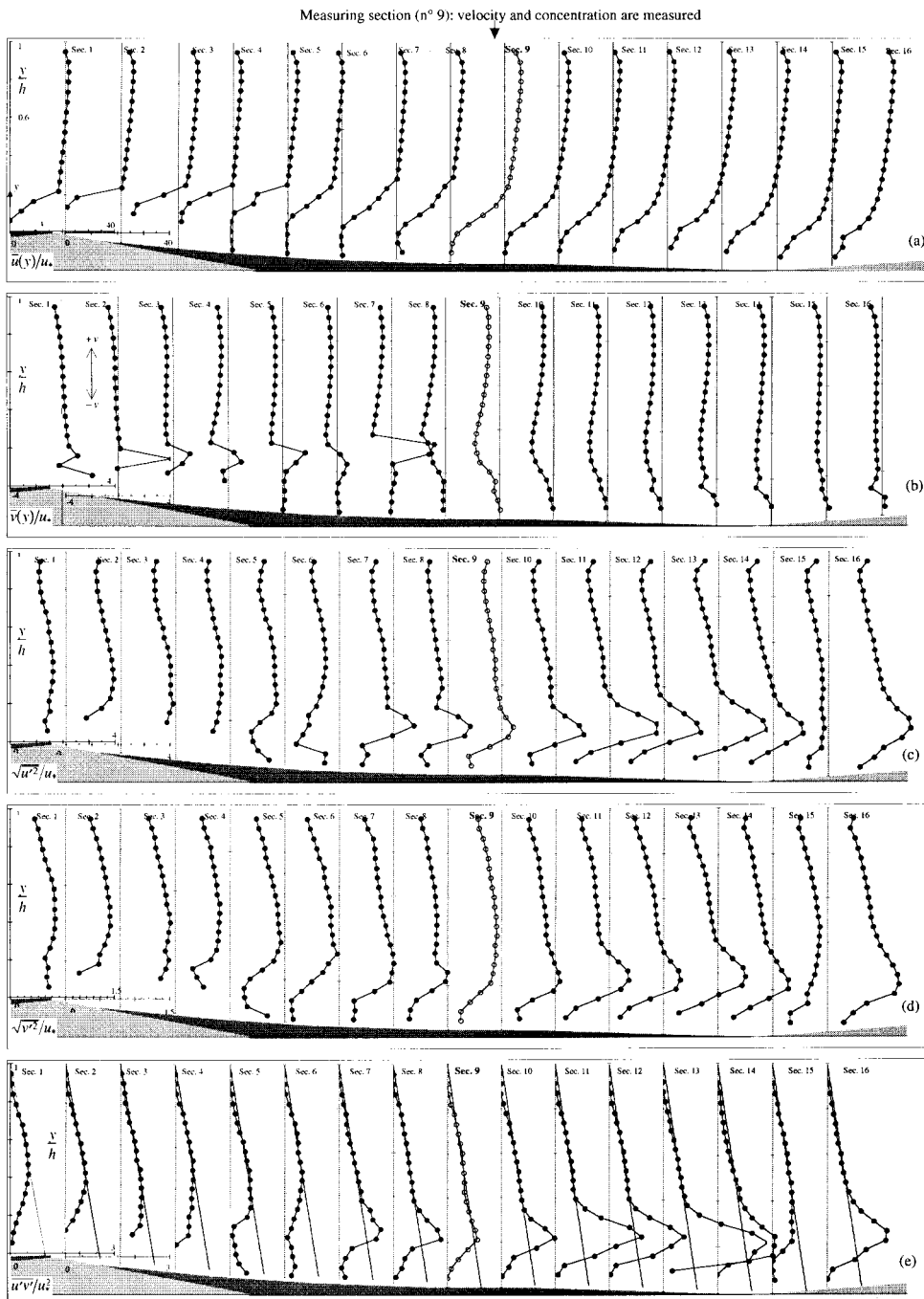


Fig. 4. a,b,c,d,e. Velocity, turbulence intensity and Reynolds stress profiles.

The dimensionless Reynolds-stress profiles (see Fig. 3c) show a clear peak in the vicinity of the bed-form crest ( $y/h \approx 0.17$ ) which was also evident in the numerical studies of Mendoza and Shen, 1990, p. 467, and of Yoon and Patel, 1996, p. 15. The fact that the Reynolds-stress profiles are close to be linear in the upper part of the flow,  $y/h > 0.5$ , is consistent with the findings of Lyn, 1993, p. 318. The Reynolds stress at the wall is considerably lower than the one at the bed-form crest. This fact illustrates the role which turbulence, thus the shear stress, will have on the particle dynamics. Sediment particles which arrive at the bed-form crest (due to previously accelerating flow) will readily remain suspended due to the high degree of turbulence in the

flow's free-shear layer. However when particles settle, they will probably remain rather long as part of the bed.

#### 4 Spatial evolution of the flow structure

For the two runs, BF\_S015 and BF\_S02, the APFP instrument has been used to measure both the velocity and concentration profiles, but only in the measuring section n° 9 (see Fig. 1). In addition, for the same hydraulic conditions as existed in run BF\_S015 the velocity field around a bed form has been measured in 16 sections, spaced at 1 [cm]. This investigation has been carried out to study the longitudinal evolution of the flow.

While the overall characteristics of the flow are given in Table 1, the characteristics of the flow evolution are summarized in Table 2 for the 16 sections investigated. The distance from the bed,  $y$ , refers to the sediment layer on bed forms. The flow depth,  $h$ , represents the distance from the top of the sediment layer to the water surface (see Fig. 1).

In Fig. 4 are plotted the dimensionless distributions of the longitudinal (a) and the vertical (b) velocity, their turbulence intensities (c, d) and the Reynolds stresses (e); the shear velocity is always taken as  $u_* \equiv u_{*t}$ .

The longitudinal velocity profiles (see Fig. 4a) seem to be strongly affected by the presence of the bed form. In some sections (from  $n^\circ 5$  to  $n^\circ 8$ ) it is even possible to observe negative values of the velocity (directed towards upstream) generated by a flow recirculation behind the bed-form crest. The vertical velocity profiles (see Fig. 4b) show negative values (velocity directed towards the bed) behind the bed-form crest. This is due to the tendency of the flow to reattach itself towards the bed downstream of the bed-form crest. The longitudinal (see Fig. 4c) and vertical (see Fig. 4d) turbulence intensity profiles show, behind the bed-form crest (from section  $n^\circ 5$  to  $n^\circ 16$ ), the presence of peaks associated with the existence of a separating shear layer. The dimensionless Reynolds-stress profiles have been plotted in Fig. 4e. Only in the upper part of the flow ( $y/h > 0.5$ ) the measured Reynolds-stress profiles follow reasonably the linear trend. Closer to the bed ( $y/h < 0.5$ ) the development of a shear layer is confirmed by the presence of peaks.

Table 2. Summary of data for run BF\_S015.

Sect.	$h$	$\delta$	$\bar{u}_c$	$U$	$Fr$	$u_* \equiv u_{*t}$	$u_{*s}$	$f$	$Re_{10^4}$	$k_s$	$u_* k_s / \nu$	$\bar{\Pi}$
	[m]	[m]	[m/s]	[m/s]	[-]	[m/s]	[m/s]	[-]	[-]	[mm]	[-]	[-]
1	0.092	0.080	0.834	0.677	0.71	0.037	0.037	0.024	6.23	0.366	13.64	0.253
2	0.092	0.083	0.839	0.651	0.67	0.032	0.037	0.020	6.19	0.089	2.87	0.268
3	0.102	0.089	0.840	0.654	0.65	0.033	0.039	0.020	6.67	0.136	4.47	0.320
4	0.105	0.092	0.832	0.612	0.60	0.034	0.039	0.024	6.42	0.397	13.31	0.335
5	0.107	0.093	0.835	0.589	0.57	0.033	0.040	0.025	6.30	0.447	14.57	0.504
6	0.107	0.093	0.823	0.585	0.57	0.038	0.040	0.033	6.26	1.541	58.24	0.517
7	0.108	0.094	0.811	0.584	0.57	0.031	0.040	0.023	6.30	0.324	10.16	0.407
8	0.109	0.095	0.811	0.598	0.58	0.030	0.040	0.020	6.52	0.113	3.36	0.555
9	0.110	0.096	0.800	0.601	0.58	0.031	0.040	0.021	6.62	0.200	6.21	0.576
10	0.111	0.097	0.799	0.595	0.57	0.030	0.040	0.021	6.60	0.171	5.17	0.723
11	0.112	0.098	0.783	0.582	0.55	0.031	0.041	0.023	6.52	0.345	10.79	0.664
12	0.113	0.099	0.781	0.577	0.55	0.031	0.041	0.023	6.52	0.361	11.24	1.007
13	0.116	0.101	0.780	0.569	0.53	0.029	0.041	0.020	6.60	0.150	4.31	1.185
14	0.115	0.100	0.778	0.578	0.54	0.029	0.041	0.020	6.65	0.151	4.42	1.100
15	0.112	0.098	0.772	0.593	0.57	0.030	0.041	0.020	6.64	0.133	3.94	0.979
16	0.110	0.096	0.774	0.595	0.57	0.031	0.040	0.022	6.55	0.264	8.26	1.032
average	0.108	0.094	0.806	0.603	0.59	0.032	0.040	0.023	6.47	0.324	10.94	0.652

The overall tendency of the flow's evolution over a bed form, as shown in Fig. 4, is rather similar to the one observed behind a bed-form crest by Nelson, McLean and Wolfe, 1993, p. 12734, McLean, Nelson and Wolfe, 1994, p. 3939 and Bennett and Best, 1995, p. 502, as well as behind a back-facing step by Etheridge and Kemp, 1978, p. 552, Nakagawa and Nezu, 1987, p. 69, and Wang and Fontijn, 1993, p. 306.

The friction factor,  $f$ , has been computed by  $f = 8(u_* / U)^2$  (see Table 2). Using the Colebrook-White formula (with the values  $a_f = 11.5$  and  $b_f = 1.5$  given by Silberman et al., 1963, pp. 97–143) the values of the equivalent bed roughness,  $k_s$ , have been calculated. Note, that  $f$  and  $k_s$  have to be considered as local values being calculated from the local estimation of the shear velocity,  $u_* \equiv u_{*t}$ . The particle Reynolds number,  $u_* k_s / \nu$ , shows that the bed is not hydraulically rough,  $u_* k_s / \nu < 70$ . The  $\bar{\Pi}$ -values have been obtained fitting the theoretical Coles' defect law to the

measured profiles, but applied only in the upper part of the flow,  $y/h > 0.5$ , to exclude the recirculation region close to the bed.

The measured longitudinal velocity profiles plotted in defect form,  $(\bar{u}_c - \bar{u})/u_*$  vs  $y/\delta$ , where  $u_c$  is the maximum velocity observed at  $y = \delta$ , are shown in Fig. 5a. Also shown is the theoretical Coles' defect law plotted using an average value of the wake strength,  $\bar{\Pi} = 0.652$  (see Table 2). A value  $\bar{\Pi} > 0.2$ , would indicate that the flow is a decelerating one (see Graf and Altinakar, 1991, p.60) being caused by the reattachment of the flow to the bed. The Coles defect law describes somehow the experimental profiles only for  $y/\delta > 0.3$ . Close to the bed,  $y/\delta < 0.3$ , the experimental points deviate strongly from the theoretical distribution; this corroborates with the observations done by Lyn, 1993, p.313. The magnitude of the averaged  $\bar{\Pi}$ -value agrees with the tendency shown experimentally by Coleman, 1981, p. 221.

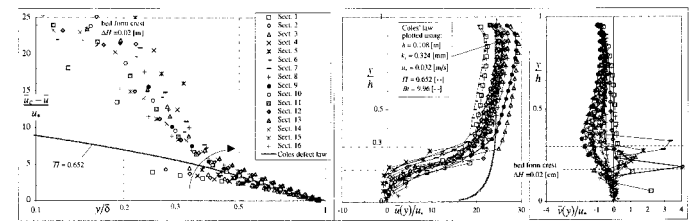


Fig. 5a,b,c. Velocity mean profiles.

In Fig. 5b are plotted all the dimensionless longitudinal mean velocities,  $\bar{u}(y)/u_*$ , against the dimensionless coordinate,  $y/h$ . Apart some scatter all the profiles are similar. The gray full line in Fig. 5b represents the Coles law plotted using the spatially averaged hydraulic parameters (see Table 2), namely:  $h = 0.108$  [m],  $k_s = 0.324$  [mm],  $u_* = 0.032$  [m/s] and  $\bar{\Pi} = 0.652$  [-]. Coles' law and the experimental profiles are very similar in the upper part of the flow,  $y/h > 0.3$ , while closer to the bed,  $y/h < 0.3$ , the presence of a recirculating region attenuates strongly the experimental profiles. Note also the presence of weak negative velocities (directed towards upstream) below the bed-form crest. These results confirm the tendency observed previously investigating only section  $n^\circ 9$  (see Fig. 2a,b).

In Fig. 5c are presented the vertical mean velocity profiles,  $\bar{v}(y)/u_*$ . Except for a few profiles (from sections  $n^\circ 1$  to  $n^\circ 7$  and close to the bed) the vertical velocities are always negative (directed towards the bed). This confirms – as shown in Fig. 2c investigating section  $n^\circ 9$  only – that behind section  $n^\circ 7$  the flow reattaches itself towards the bed.

In Fig. 6a are presented the Reynolds-stress profiles compared with the theoretical linear distribution,  $\bar{u}'v'(y) = u_*^2(1 - y/h)$ . In the upper part of the flow ( $y/h > 0.4$ ), the Reynolds stress distribution seems to be linear; this result is consistent with the findings of Lyn, 1993, pp. 318. Close to the bed, the measured Reynolds-stress profiles are perturbed; in particular pronounced peaks are observed which can be associated to the development of a shear layer behind the bed-form crest caused by a separated flow.

In Fig. 6b,c the longitudinal,  $\sqrt{\bar{u}'^2}/u_*$ , and the vertical,  $\sqrt{\bar{v}'^2}/u_*$ , component of the turbulence intensity are presented. These intensity profiles are self similar and comparable to the ones measured in suspension flow over plane bed (see gray lines). An important

difference is represented by the peak values, caused by the developing shear layer, detected close to the bed ( $y/h < 0.4$ ) in case of flow over bed forms. Again, this is qualitatively consistent with the measurements of Lyn, 1993, p. 316, and of Kobayashi et Togashi, 1993, p. 133. The full lines in Fig. 6b,c represent the universal expression of the components of the turbulence intensity (in clear water) proposed by Nezu and Nakagawa, 1993, p. 53, using the empirical coefficients obtained by Kironoto, 1992, p. 3.18. The longitudinal component of the turbulence intensity in both type of suspension flow (over a plane bed – gray patterns – and over bed forms – experimental symbols) seems to be slightly enhanced. On the other hand, the vertical component of the turbulence intensity seems to be suppressed over the entire flow depth and especially very close to the bed ( $y/h < 0.1$ ).

By using the data displayed in Figs. 4 contour plots were obtained. In Fig. 7a,b the contour plots of the longitudinal and vertical mean velocity are presented. The contour plot of the longitudinal velocity,  $\bar{u}$ , shows that between sections n° 1 and n° 8 the iso-velocity lines are closely spaced, reflecting the strong vertical gradient of the velocity profiles. Behind section n°8 the iso-velocity lines become more distant. The contour plot

of the vertical velocity,  $\bar{v}$ , shows that between sections n° 1 and n° 7 and close to the bed, the direction of the flow is towards the surface, while behind section n° 7 the direction of the flow is towards the bed. This implies that the reattachment of the flow towards the bed starts behind section n° 8. The contour plot of the velocity vectors,  $\vec{V}(\bar{u}, \bar{v})$ , is given with Fig. 7c. It reveals the presence of a weak reverse flow between sections n° 4 and n° 7 behind the bed-form crest, the separation of the flow between sections n° 2 and n° 8 and finally the reattachment of the flow to the bed behind section n° 8.

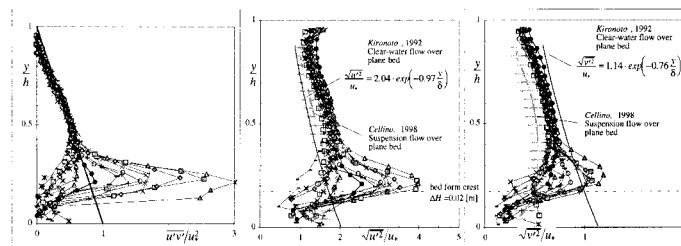


Fig. 6. a,b,c. Dimensionless Reynolds-stress, longitudinal and vertical turbulence intensity profiles

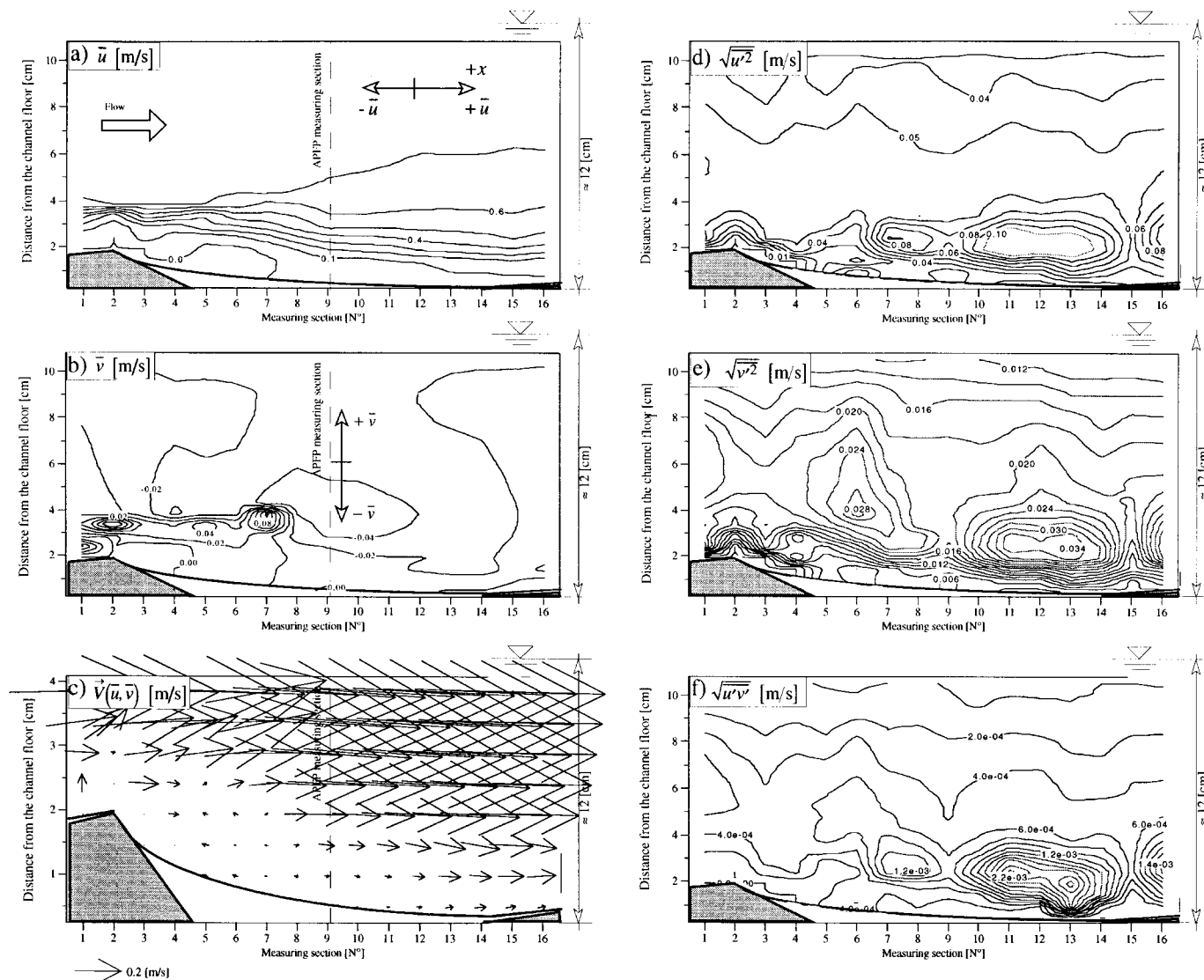


Fig. 7. Contour plots of a) Longitudinal mean velocity, b) Vertical mean velocity, c) Vector plot of mean velocity, d) Longitudinal turbulent fluctuations, e) Vertical turbulent fluctuations, f) Reynolds stress.

In Fig. 7d,e are given the contour plots of the longitudinal and vertical turbulence intensity. The presence of the bed forms generates zones of high turbulence intensity between sections n°8 and n° 16, where the flow reattaches itself towards the bed. The contour plots of the Reynolds stress, given in Fig. 7f, show a strong enhancement between the sections n° 8 and n° 16, notably close to the bed. The enhancement of both turbulence intensity and Reynolds stress is caused by the developing shear layer due to the separated flow. These results are consistent with numerical and experimental observations made by Yoon and Patel, 1996, p. 13, by Lyn, 1993, p. 318 and by Bennett and Best, 1995 p. 502; for flow over a backward-facing step, Etheridge and Kemp, 1978, p. 555 and Nakagawa and Nezu, 1987, p. 76, made similar observations.

Subsequently, the mean transversal vorticity,  $\omega_z$ , has been computed from the mean longitudinal and vertical velocity component:

$$\omega_z = \frac{1}{2} \left( \frac{\partial \bar{u}}{\partial y} - \frac{\partial \bar{v}}{\partial x} \right) \quad (3)$$

The derivative terms,  $\partial \bar{u} / \partial y$  and  $\partial \bar{v} / \partial x$ , have been calculated using a center-finite difference approximation. The corresponding contours of constant  $\omega_z$  are plotted in Fig. 8a. These contour lines show that a high positive (clockwise) vorticity region develops above the bed-form crest, whose magnitude diminishes towards the downstream. A low negative vorticity region develops at the bed-form crest up to the reattachment point at section n° 8. Also indicated are the upper,  $y_{UV}$ , and lower,  $y_{DV}$ , limit of the high vorticity region.

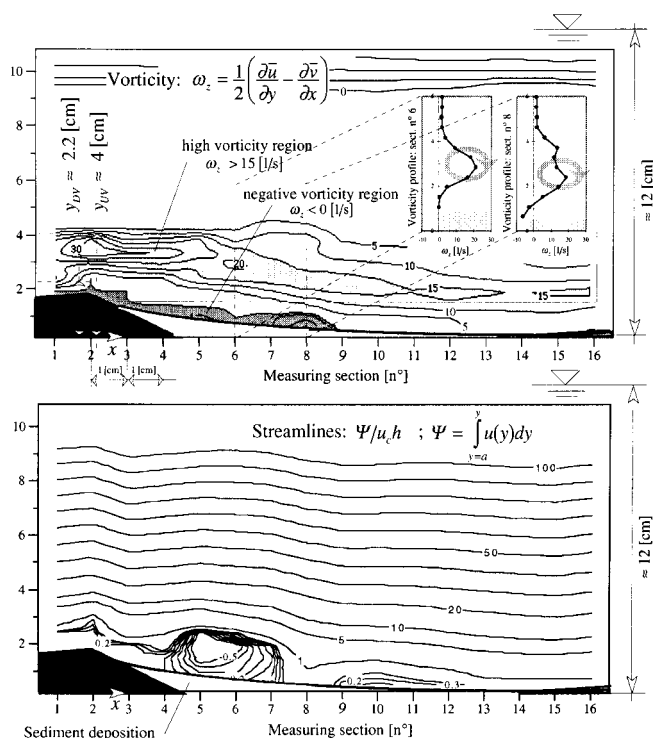


Fig. 8. a,b. Contour plot of the vorticity and streamlines

Mean streamlines have been constructed from the velocity profiles in form of lines of constant  $\Psi / (u_c \cdot h)$ , where the stream function is given by:

$$\Psi = \int_a^y \bar{u}(y) \cdot dy$$

This is plotted in Fig. 8b, where around the section n° 6, a reverse-flow region is evident, delimited by  $\Psi = 0$ . Reattachment of the flow is reached at the section n° 8.

## 5 Concentration measurements

As was explained earlier, concentration measurements could only be performed at one single section, notably section n° 9, since the APFP instrument could only be operated in a fixed position.

The mean concentration profiles,  $\bar{c}_s^m(y)$  – measured with the suction method – as well as the profiles of the dimensionless fluctuating sediment concentration,  $\sqrt{c_s'^2} / \bar{c}_{sa}$  – measured with the APFP instrument – are plotted in Fig. 9a,b. The reference concentration,  $\bar{c}_{sa}$ , evaluated at  $a = 0.05 \cdot h$  with the suction method (see Table 1) has been used as a scaling parameter; it represents the largest concentration of sediments transported in suspension. The depth-averaged concentration,  $C_s^m$ , is obtained integrating the mean concentration profile,  $\bar{c}_s^m(y)$ , over the flow depth. The dimensionless fluctuating concentration profiles,  $\sqrt{c_s'^2} / \bar{c}_{sa}$ , (see Fig. 9b) have their maximum values close to the bed ( $y/h < 0.25$ ); in the upper part of the flow ( $y/h > 0.25$ ) the fluctuating concentrations decrease quite rapidly. The vertical distribution of mean concentration (see Fig. 9a) and fluctuating concentration (see Fig. 9b) are comparable to the ones measured in plane-bed suspension flows (gray symbols in Fig. 9a,b). The profiles of the sediment flux,  $c_s \cdot v'$  – obtained with the APFP and normalized with their values at the bed – are plotted on Fig. 10. While some scatters is evident, in both cases a peak close to the height of the bed-form crest is noticeable. Apart of these peaks the tendency is similar to the one observed in comparable plane-bed suspension flows (gray symbols).

The momentum-,  $\epsilon_m(y)$ , as well as the sediment-diffusion coefficient,  $\epsilon_s(y)$ , are evaluated from the measured data set – obtained with the APFP instrument – using their definition given with eq. 4.

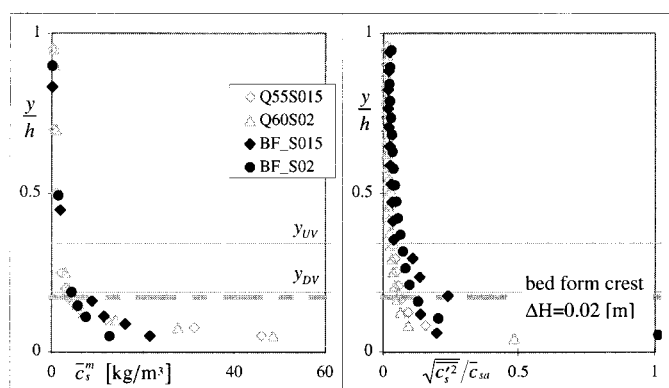


Fig. 9. a,b. Vertical mean and fluctuating concentration profiles.

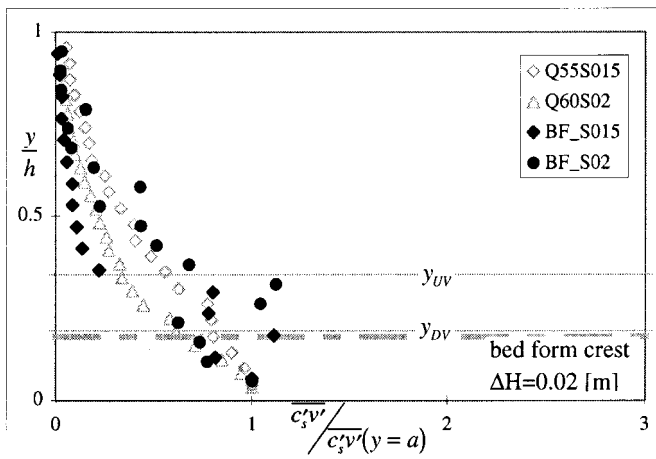


Fig. 10. Sediment flux normalized with its value at the bed.

The dimensionless momentum,  $\varepsilon_m/(u_*h)$ , and sediment,  $\varepsilon_s/(u_*h)$ , diffusion coefficient profiles are plotted in Fig. 11a,b. For the first (BF\_S015 in Fig. 11a) and for the second run (BF\_S02 in Fig. 11b) the dimensionless momentum- and sediment-diffusion coefficient profiles show in both cases a peak close to the same location, namely at  $y/h \approx 0.3$ , situated above the bed-form crest. In the case of suspension flows over a comparable plane bed (see gray points in Fig. 11a,b) no pronounced peak is distinguishable.

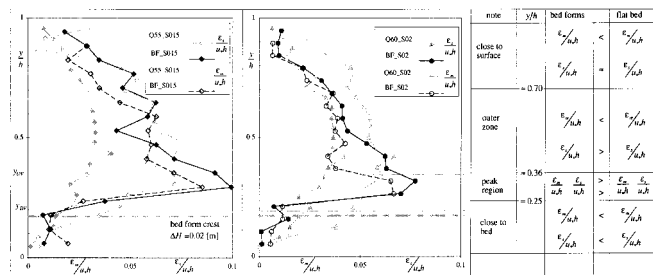


Fig. 11. a,b: Dimensionless sediment- and momentum- diffusion coefficient profiles.

The dimensionless sediment diffusion coefficients,  $\varepsilon_s/(u_*h)$ , measured in flows over bed forms, are larger – between  $0.25 < y/h < 0.70$  – than the ones measured in suspension flows over plane bed. This means that the particles are diffused more efficiently by the high turbulence region generated by the bed-form. Close to the water surface –  $y/h > 0.70$  – the coefficients are similar probably because the effect of the bed forms becomes negligible. Close to the bed –  $y/h < 0.25$  – the sediment diffusion coefficients measured in suspension flows over bed forms fall to zero more rapidly becoming smaller than the ones measured in flows over plane bed. This effect is related to the small velocities, turbulence intensities and shear stress measured close to the bed.

The dimensionless momentum diffusion coefficients,  $\varepsilon_m/(u_*h)$ , measured in flows over bed-forms, are smaller than the ones measured in flows over plane bed in the upper region of the flow (above the upper level of the turbulent region,  $y_{UV}$  or  $y/h \approx 0.36$ ).

Below this level, where the peaks have been observed, the coefficients measured over bed forms are slightly larger than the ones measured in plane-bed flows. Close to the bed –  $y/h < 0.25$  – they become smaller, falling to zero more rapidly than the ones measured over plane bed. Such a tendency was also reported by Lyn, 1993, p. 321, and by Thorne et al., 1996, p.351.

The enhancement of the sediment-diffusion coefficients over a large part of the flow depth and the partial suppression of the momentum-diffusion coefficients can be interpreted as being due to the effect of the shear layer – generated by the bed-form crest – that diffuses more efficiently the particles in the flow and that partially inhibits the diffusion of momentum.

The ratio of the sediment- and momentum-diffusion coefficient defines the  $\beta(y)$ -values, given with eq. 4; it is shown in Fig. 12a,b. Also shown is the depth-averaged value,  $\bar{\beta}_{APFP}$ , being close to the unity (see Table 1). For suspension flows over plane bed (gray symbols), it has been shown (see Cellino, 1998, §3 and Appendix B) that the experimental  $\beta(y)$ -values – obtained using the APFP instrument – are always smaller than unity. Such an increase is mainly due to the effect of the high turbulence region – generated by the bed-form crest – when the sediment diffusion coefficient is considerably enhanced and the momentum diffusion coefficient is suppressed, leading to an augmentation of the  $\bar{\beta}$ -values.

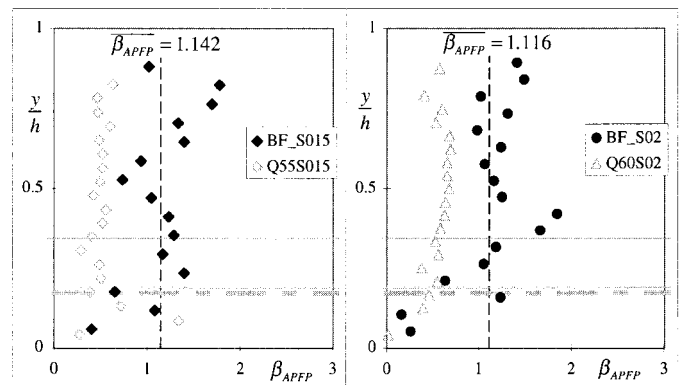


Fig. 12. a,b. Profiles of  $\beta$ -values

The concentration profiles – measured with the suction method – are shown for both runs in Fig. 13a,b, using black symbols. For sake of comparison the Rouse equation is shown, using the “theoretical”  $\bar{\beta}$ -value of  $\bar{\beta} = 1$  (full line). Also shown is the Rouse equation plotted using the  $\bar{\beta}_{APFP}$ -values (obtained with the diffusion coefficients, dashed line) as well as the best-fit  $\bar{\beta}_{SM}$ -values (obtained by best fitting the Rouse equation, eq. 2, to the vertical concentration profiles measured using the suction method, dotted line, see Cellino, 1998, Appendix B). The agreement between the measured concentration profiles (black symbols) and the one using the  $\bar{\beta}_{APFP}$ -values (dashed line) is in both cases satisfactory.

With the present experiments, we believe to shed some light on the long-standing argument (see Graf, 1984, p. 174) whether or not the  $\bar{\beta}$ -value is larger or smaller than unity. For the same sediment particles – to be considered as fine particles,  $v_{ss}/u_* < 0.5$  – the  $\bar{\beta}$ -value is  $\bar{\beta} < 1$  for flow over a plane bed, however

in the presence of a bed form, the  $\bar{\beta}$ -value is  $\bar{\beta} > 1$ . This would in a way explain the field data obtained on the Rio Grande river reported by Nordin and Dempster, 1963, where the presence of a bed forms is undeniable and consequently the reported  $\bar{\beta}$ -values are rather large,  $\bar{\beta} > 1$ . Note, that data from the Enoree river reported by Anderson, 1942, and from the Niobrara river by Colby et al., 1955, (see Graf, 1984, p. 177) show the very same tendency.

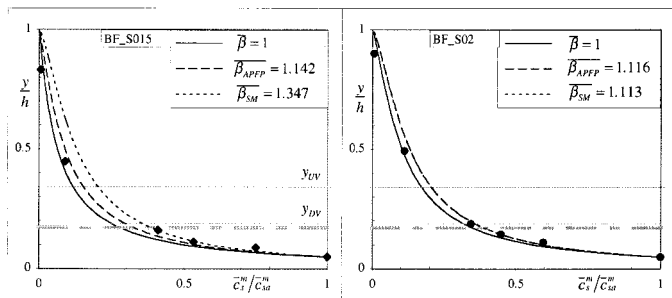


Fig. 13. a,b. Vertical mean concentration profiles

## 6 Conclusions

Suspension flows over bed forms have been investigated using a non-intrusive sonar APFP instrument. The measurements were performed with the flow in capacity (saturation) condition. In the main part of the paper, we studied the diffusion coefficients of the flow over a bed form. Due to the limitation in the use of the APFP instrument to measure the concentration profiles, only one single section – section n° 9 – could be investigated. The longitudinal and vertical mean velocity profiles, measured in this section, confirms the separation of the flow. The longitudinal and vertical components of the turbulence intensity as well as the Reynolds-stress profiles show pronounced peaks close to the bed-form crest; this is in agreement with the flow structure shown in another part of the paper. The vertical mean concentration profiles, measured at this section – using the suction method – as well as the fluctuating concentration profiles – measured using the APFP instrument – are similar to the ones measured in suspension flow over plane bed (see Fig. 9a,b). The sediment fluxes profiles – measured with the APFP instrument – show peaks located close to the bed-form crest (see Fig. 10). Apart of these peaks, the tendency is rather similar to the one observed in comparable suspension flow over plane bed.

The dimensionless sediment diffusion coefficient profiles,  $\varepsilon_s(y)$ , compared to the ones measured in suspension flow over plane bed, are enhanced over a large portion of the flow depth. On the contrary, the momentum diffusion coefficient profiles,  $\varepsilon_m(y)$ , are partially suppressed (see Fig. 11a,b). This can be interpreted as being due to the effect of the shear layer, generated by the bed-form crest, that diffuses more efficiently the particles in the flow, but partially inhibits the diffusion of momentum.

The depth-averaged  $\bar{\beta}(y)$ -values measured experimentally (being calculated as the ratio of the sediment and the momentum diffusion coefficients), are larger than unity,  $\bar{\beta}_{APFP} > 1$  (see

Fig. 12a,b). In the same figure they are compared to the values measured in a comparable suspension flow over plane bed; here it is evident that  $\bar{\beta}_{APFP} < 1$  (see Cellino, 1998). The agreement between the measured concentration distributions, using the suction method, and the Rouse equation, eq. 4, using the  $\bar{\beta}_{APFP}$ -values measured using the APFP instrument, is considered to be very good (see Fig. 13a,b).

Thus, the presence of bed forms affects the suspension flows, leading to larger  $\bar{\beta}$ -value,  $\bar{\beta} > 1$ , than the ones observed in suspension flow over plane bed, where  $\bar{\beta} < 1$ .

In another part of the paper the spatial evolution of the flow structure was studied. The longitudinal and vertical mean velocity profiles, measured in sections located between two bed forms and close to the bed-form crest, show the separation of the flow and its successive reattachment to the bed (see Fig. 4a,b and 5a,b,c). The longitudinal and vertical components of the turbulence intensity as well as the Reynolds-stress profiles show pronounced peaks close to the bed-form crest,  $y/h \approx 0.17$  (see Fig. 4c,d,e and 6a,b,c). These peaks are generated by the developing shear layer caused by the separation of the flow. The resulting vorticity contour lines show that a high positive (clockwise) vorticity region develops on top of the bed-form crest; its magnitude diminishes towards the downstream. Underneath and beginning at the bed-form crest a weak negative (anti-clockwise) vorticity region develops; it extends up to the reattachment of the flow (see Fig. 8A).

## 7 Acknowledgements

This work was made possible by the support of the Swiss National Science Foundation, grant number 20-39495.93. The use of the APFP instrument was greatly facilitated by the help of D. Hurther, U. Lemmin, and C. Shen of our laboratory. The discussions we had with D. Lyn are appreciated.

## 8 References

- BENNETT, S.J. and BEST, J.L. (1995). "Mean flow and turbulence structure over fixed, two-dimensional dunes: implications for sediment transport and bedform stability." *Sedimentology*, vol. 42, pp. 491–513.
- CELLINO, M. and GRAF, W.H., (1997) "Measurements of suspension flow in open channels", *Proceedings of XXVII IAHR Congress.*, vol. 1, pp. 179–184, San Francisco.
- CELLINO, M. (1998). "Suspension Flow in Open Channel." Doctoral dissertation n° 1824, Ecole Polytechnique fédérale de Lausanne.
- COLEMAN, N.L. (1970). "Flume Studies of the Sediment Transfer Coefficient." *Water Resour. Res.*, Vol. 6, N° 3, pp. 801–809.
- COLEMAN, N.L. (1981). "Velocity profiles with suspended sediment." *J. Hydr. Res.*, vol. 19, N° 3, pp. 211–229.
- ETHERIDGE, D.W. and KEMP, P.H. (1978). "Measurements of turbulent flow downstream of a rearward-facing step" *J. Fluid Mech.*, vol. 86, N° 3, pp. 545–566.
- GRAF, W.H. (1984). *Hydraulics of Sediment Transport*. Water Resource Publications, Littleton, CO, USA.
- GRAF, W.H. and ALTINAKAR, M.S. (1991). *Hydrodynamique*. Eyrolles, Paris, F.
- JOBSON, H.E. and SAYRE, W.W. (1970). "Vertical Transfer in Open Channel Flow." *Proc., Am. Soc. Civil Engrs.*, vol. 96, N° HY3, pp. 703–724.

- KIRONOTO, B. (1992). "Turbulence characteristics of non-uniform Flow in rough Open-channel." Doctoral dissertation N° 1094, Ecole Polytechnique Fédérale de Lausanne.
- KOBAYASHI, T. And TOGASHI, S. (1993). "Comparison of turbulence models applied to backward-facing step flow by LES data base" in Engineering Turbulence Modelling and Experiments 2, W. RODI and F. MARTELLI, Elsevier.
- LHERMITTE, R. and LEMMIN, U. (1994). "Open-Channel Flow and Turbulence Measurements by High-Resolution Doppler Sonar." *J. Atmospheric and Oceanic Tech.*, vol. 11, N° 5, pp. 1295–1308.
- LYN, D.A. (1988). "A similarity approach to turbulent sediment-laden flows in open channels." *J. Fluid Mech.*, Vol. 193, pp. 1–26.
- LYN, D.A. (1993). "Turbulence Measurements in Open-Channel Flows over Artificial Bed Forms." *J. Hydr. Engr.*, vol. 119, N° 3, pp. 306–326.
- MCLEAN, S.R., NELSON, J.M. and WOLFE, S.R. (1994). "Turbulence structure over two-dimensional bed forms: Implications for sediment transport." *J. Geophysical Res.*, vol. 99, n° C6, pp. 12729–12747.
- MENDOZA, C. and SHEN, H.W. (1990). "Investigation of Turbulent Flow over Dunes." *J. Hydr. Eng.*, vol. 116, N° 4, pp. 459–477.
- NAKAGAWA, H. and NEZU, I. (1987). "Experimental investigation on turbulent structure of backward-facing step flow in an open channel." *J. Hydr. Res.*, vol. 25, N° 1, pp. 67–88.
- NELSON, J.M., MCLEAN, S.R. and WOLFE, S. R. (1993). "Mean Flow and Turbulence Fields over two-dimensional Bed Forms." *Water Resour. Res.*, vol. 29, N° 12, pp. 3935–3953.
- NEZU, I. and NAKAGAWA, H. (1993). *Turbulence in open-channel flows*. A. A. Balkema, Rotterdam, NL.
- NORDIN, C.F. and DEMPSTER, G.R. (1963). "Vertical Distribution of Velocity and Suspended Sediment Middle Rio Grande New Mexico." US Geol. Survey; Professional Paper 462-B, Washington, DC, USA.
- SHEN, W. (1997). "An acoustic instantaneous sediment flux profiler for turbulent flow." Doctoral dissertation, No. 1630, Ecole Polytechnique Fédérale, Lausanne, CH.
- SHEN, W. and LEMMIN, U. (1996). "Ultrasonic measurements of suspended sediments. A concentration profiling system with attenuation compensation." *Meas. Sci. Tecn.*, vol. 7, pp. 1191–1194
- SILBERMAN, E. et al. (1963). "Friction Factors in Open Channels." *Proc., Am. Soc. Civil Engrs.*, vol. 90 HY1, USA.
- SUMER, B.M. et al. (1996). "Velocity and Concentration Profiles in Sheet-Flow Layer of Movable Bed." *J. Hydr. Engr.*, vol. 122, N°. 10, pp. 549–558.
- THORNE, P.D. et al. (1996). "Observation of Near-bed Suspended Sediment Turbulence Structures using Multifrequency Acoustic Backscattering" in: *Coherent Flow Structures in Open Channels*, Wiley & Sons Ltd., Chichester, UK.
- WANG, X. and FONTJIN, H.L. (1993). "Experimental study of the hydrodynamic forces on a bed element in an open channel with a backward-facing step" *J. Fluids and Struct.*, vol. 7, pp. 299–318.
- YOON, J.Y. and PATEL, V.C. (1996). "Numerical model of turbulent flow over sand dune." *J. Hydr. Engr.*, vol. 122, N° 1, pp. 10–18.